



Thermal behaviour of malonic acid, sodium malonate and its compounds with some bivalent transition metal ions

F.J. Caires, L.S. Lima, C.T. Carvalho*, R.J. Giaggio, M. Ionashiro

Instituto de Química, Universidade Estadual Paulista, CP 355, 14801-970 Araraquara, SP, Brazil

ARTICLE INFO

Article history:

Received 2 July 2009

Received in revised form 10 August 2009

Accepted 13 August 2009

Available online 1 September 2009

Keywords:

Bivalent transition metals

Malonates

Thermal behaviour

ABSTRACT

Characterization, thermal stability and thermal decomposition of transition metal malonates, $MCH_2C_2O_4 \cdot nH_2O$ ($M = Mn(II), Fe(II), Co(II), Ni(II), Cu(II), Zn(II)$), as well as, the thermal behaviour of malonic acid ($C_3H_4O_4$) and its sodium salt ($Na_2CH_2C_2O_4 \cdot H_2O$) were investigated employing simultaneous thermogravimetry and differential thermal analysis (TG-DTA), differential scanning calorimetry (DSC), infrared spectroscopy, TG-FTIR system, elemental analysis and complexometry. The dehydration, as well as, the thermal decomposition of the anhydrous compounds occurs in a single step. For the sodium malonate the final residue up to 700 °C is sodium carbonate, while the transition metal malonates the final residue up to 335 °C (Mn), 400 °C (Fe), 340 °C (Co), 350 °C (Ni), 520 °C (Cu) and 450 °C (Zn) is $Mn_3O_4, Fe_2O_3, Co_3O_4, NiO, CuO$ and ZnO , respectively. The results also provided information concerning the ligand's denticity, thermal behaviour and identification of some gaseous products evolved during the thermal decomposition of these compounds.

© 2009 Elsevier B.V. All rights reserved.

1. Introduction

The interest in the thermal study of compounds of malonate stems from the great number of applications of malonate ions that have been reported in the literature. The malonate ions are employed in the controlled assembly of malonates and ions into strategies for supramolecular synthesis and crystal engineering purposes [1,2], for designing complexes with desired magnetic properties [2,3] and so on.

Preparation and investigation of several metal-ion malonates have also been investigated in the solid-state using thermoanalytical techniques, X-ray diffractometry and infrared spectroscopy. The papers published are concerned with the thermal dehydration of alkali metal malonate [4], thermal decomposition of malonic acid and alkali metal malonate [5], TG-DTA analyses of europium oxalate and malonate [6], preparation and thermal dehydration manganese (II) dicarboxylate hydrates [7], thermal behaviour of alkaline earth metal malonates [8], a kinetic and mechanistic study of the thermal decomposition of nickel malonate [9], kinetic and thermodynamic studies of the non-isothermal decompositions of nickel and cobalt malonates dihydrate and nickel and cobalt hydrogen malonates dihydrate [10,11], isothermal and non-isothermal decomposition of zinc malonates [12] and thermal decomposition of transition metal malonates [13].

In this paper, the object of the present research was to investigate the thermal behaviour of malonic acid and its sodium salt, as well as to prepare solid-state compounds of some bivalents transition metal ions (i.e. Mn, Fe, Co, Ni, Cu and Zn) with malonate and to characterize and to investigate by means of complexometry, elemental analysis, X-ray powder diffractometry, infrared spectroscopy, simultaneous thermogravimetry and differential thermal analysis (TG-DTA) and differential scanning calorimetry (DSC). The thermal studies were performed in dynamical air atmosphere. The results associated with these compounds are discussed in connection with the paper of Ref. [13].

2. Experimental

The malonic acid, $C_3H_4O_4$, with 99% purity and the sodium malonate monohydrated, $Na_2CH_2C_2O_4 \cdot H_2O$, 99.6% were obtained from Sigma.

Carbonates of Mn(II), Fe(II), Co(II), Ni(II), Cu(II) and Zn(II) were prepared by adding slowly with continuous stirring the saturated sodium hydrogen carbonate solution to the corresponding metal chloride or sulphate for iron and copper solutions until total precipitation of the metal ions. The precipitates were washed with distilled water until the elimination of chloride or sulphate ions (qualitative test with $AgNO_3/HNO_3$ solution for chloride ions or $BaCl_2$ solution for sulphate ions) and maintained in aqueous suspension. To avoid oxidation of Fe (II), all the solutions, as well as the water employed for washing the precipitate were purged with nitrogen gas and the system maintained without contact with air.

* Corresponding author. Tel.: +55 16 3301 6617; fax: +55 16 3322 7932.
E-mail address: ctc.1975@yahoo.com.br (C.T. Carvalho).

Solid-state Mn(II), Fe(II), Co(II), Ni(II), Cu(II) and Zn(II) compounds were prepared by mixing the corresponding metal carbonates maintained in aqueous suspension with malonic acid, in slight excess. The aqueous suspension was heated slowly up to near ebullition, until total neutralization of the respective carbonates. Thus, the aqueous solutions of the respective metal malonates were evaporated to near dryness in water bath and washed with ethanol to eliminate the malonic acid in excess. The compounds were dried in air and kept in a desiccator over anhydrous calcium chloride.

In the solid-state compounds, metal ions, hydration water and malonate contents were determined from TG curves. The metal ions were also determined by complexometry with standard EDTA solution [14,15] after igniting the compounds to the respective oxides and their dissolution in hydrochloric acid solution.

Carbon and hydrogen contents were determined by microanalytical procedures, with an EA 1110 CHNS-O Elemental Analyser from CE Instruments.

X-ray powder patterns were obtained using a Siemens D-5000 X-ray diffractometer, employing $\text{CuK}\alpha$ radiation ($\lambda = 1.541 \text{ \AA}$) and a setting of 40 kV and 20 mA.

The attenuate total reflectance infrared spectra for sodium malonate, as well as for its metal-ion compounds were run on a Nicolet iS10 FTIR spectrophotometer, using an ATR accessory with Ge window.

Simultaneous TG-DTA and DSC curves were obtained with two thermal analysis system, model SDT 2960 and DSC Q10, both from TA Instruments. The purge gas was an air with a flow rate of 100 mL min^{-1} for TG-DTA and 50 mL min^{-1} for DSC experiments. A heating rate of $20 \text{ }^\circ\text{C min}^{-1}$ was adopted, with samples masses about 7 mg for TG-DTA and 2 mg for DSC runs. Alumina and aluminium crucibles, the latter with perforated cover, were used for TG-DTA and DSC, respectively.

The measurements of the gaseous products were carried out using a Thermogravimetric Analyzer Mettler TG-DTA coupled to a FTIR spectrophotometer Nicolet with gas cell and DTGS KBr detector. The furnace and the heated gas cell ($250 \text{ }^\circ\text{C}$) were coupled

through a heated ($T=200 \text{ }^\circ\text{C}$) 120 cm stainless steel line transfer with diameter 0.3 mm both purged with dry air (50 mL min^{-1}). The FTIR spectra were recorded with 32 scans per spectrum at a resolution of 4 cm^{-1} .

3. Results and discussion

The TG-DTA curves and IR spectrum of the gases released during the thermal decomposition of malonic acid are shown in Fig. 1(a and b). The TG curve shows mass loss in a single step between 145 and $215 \text{ }^\circ\text{C}$, and the corresponding DTA curve shows three thermal events. The first endothermic peak at $110 \text{ }^\circ\text{C}$ is due to the solid phase transition, which was confirmed by X-ray powder diffraction as shown in Fig. 1(c and d). The second and third endothermic peaks at 145 and $215 \text{ }^\circ\text{C}$ are attributed to the melting and thermal decomposition of malonic acid, respectively. The thermal decomposition of this acid occurs with decarboxylation followed by the formation of acetic acid, which was monitored and identified mostly on basis of their FTIR reference available on NICOLET libraries, as shown in Fig. 1(b).

For the sodium malonate monohydrated the TG-DTA curves, Fig. 2, show mass losses in two steps and thermal events corresponding to these losses or due to physical phenomenon. The first mass loss between 110 and $180 \text{ }^\circ\text{C}$, corresponding to an endothermic peak at $130 \text{ }^\circ\text{C}$ (DTA) is due to dehydration. The anhydrous compound is stable up to $330 \text{ }^\circ\text{C}$ and between 330 and $450 \text{ }^\circ\text{C}$ the thermal decomposition occurs in a single step with the formation of sodium carbonate. In this step the DTA curve shows a small endothermic at $342 \text{ }^\circ\text{C}$, followed by a large exothermic peak at $465 \text{ }^\circ\text{C}$ with shoulder at $420 \text{ }^\circ\text{C}$, attributed to the fusion and oxidation of organic matter, respectively.

The analytical and thermoanalytical (TG) data for the synthesized compounds are shown in Table 1. These results establish the stoichiometry of these compounds, which are in agreement with general formula: $\text{MC}_3\text{H}_2\text{O}_4 \cdot n\text{H}_2\text{O}$, where M represents Mn(II), Fe(II), Co(II), Ni(II), Cu(II) and Zn(II), $\text{CH}_2\text{C}_2\text{O}_4$ is malonate and $n = 2$ (Co, Ni, Cu, Zn) or 2.5 (Mn and Fe).

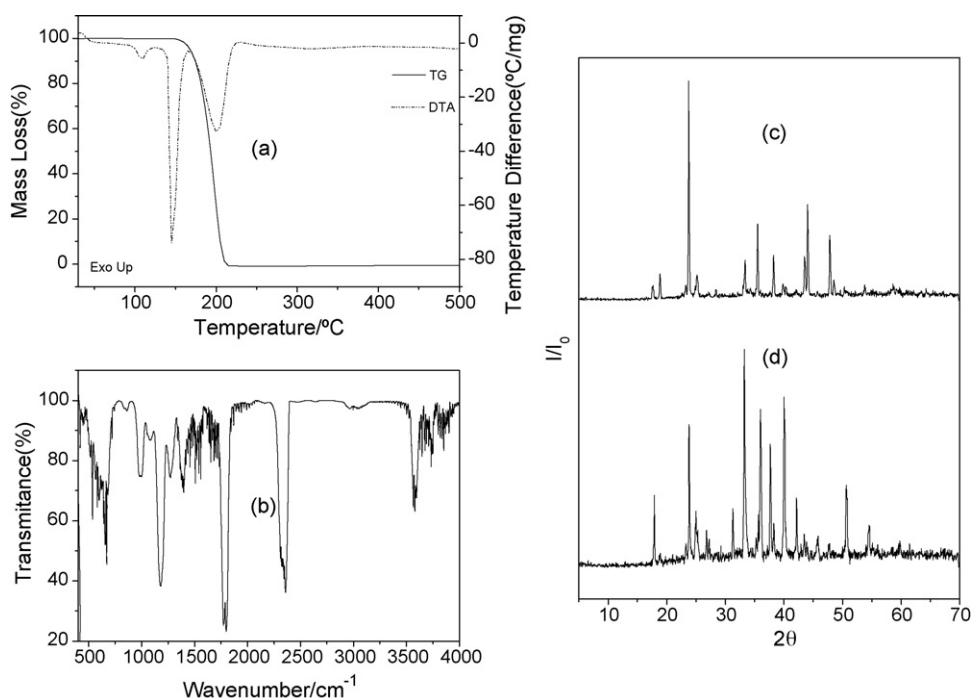


Fig. 1. Study of thermal behaviour of malonic acid: (a) simultaneous TG-DTA curves ($m = 10.744 \text{ mg}$), (b) IR spectrum of the gases released during the decomposition of malonic acid, (c) X-ray powder diffraction pattern and (d) X-ray powder diffraction pattern of the malonic acid heated until $125 \text{ }^\circ\text{C}$.

Table 1
Analytical data for the $\text{MC}_3\text{H}_2\text{O}_4 \cdot n\text{H}_2\text{O}$ compounds.

Compound	Metal oxide (%)			L (lost) (%)		H_2O (%)		C (%)		H (%)		Final residue
	Calcd.	EDTA	TG	Calcd.	TG	Calcd.	TG	Calcd.	E.A.	Calcd.	E.A.	
MnL.2.5H ₂ O	37.75	37.97	37.55	39.95	40.31	22.30	22.14	17.83	17.96	3.50	3.31	Mn ₂ O ₄
FeL.2.5H ₂ O	39.34	39.21	39.08	38.46	39.05	22.20	21.87	17.75	17.83	3.48	3.39	Fe ₂ O ₃
CoL.2H ₂ O	40.74	40.19	40.44	40.97	41.58	18.29	17.98	18.29	18.59	3.08	3.03	Co ₃ O ₄
NiL.2H ₂ O	37.96	38.12	37.76	43.73	43.69	18.31	18.55	18.31	18.25	3.08	3.12	NiO
CuL.2H ₂ O	39.45	39.10	39.06	42.68	43.31	17.87	17.63	17.87	17.60	3.01	3.05	CuO
ZnL.2H ₂ O	39.99	40.28	39.75	42.30	42.70	17.71	17.55	17.71	17.54	2.98	3.09	ZnO

L = malonate.

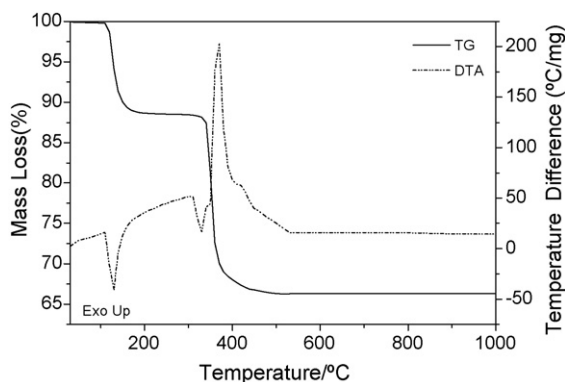


Fig. 2. Simultaneous TG-DTA curves of the sodium malonate ($m = 14.786$ mg).

The X-ray diffraction powder patterns (Fig. 3) show that all the compounds have crystalline structure and the crystallinity of these compounds follow the order: Mn > Zn > Ni > Cu > Fe.

The difference in the crystallinity of these compounds, must be probably due to the solubility of each compound and the velocity of the evaporation which was not controlled.

The XRD patterns of the compounds, when compared with patterns in ICDD data [16], are in agreement for the Mn(II), Co(II), Ni(II) and Zn(II) compounds, and in disagreement for the Fe(II) and Cu(II) ones. This disagreement, probably, is due manner as these compounds were prepared.

The attenuated total reflectance spectroscopic data on malonate and its compounds with the metal ions considered in this work are shown in Table 2. The investigation was focused mainly within

Table 2

Spectroscopic data for sodium malonate ($\text{Na}_2\text{CH}_2\text{C}_2\text{O}_4$) and compounds with some bivalent metal ions.

Compound	$\nu_{\text{as}}(\text{COO}^-)$ (cm^{-1})	$\nu_{\text{sym}}(\text{COO}^-)$ (cm^{-1})	$\Delta\nu$ ($\nu_{\text{as}} - \nu_{\text{sym}}$)
$\text{Na}_2\text{L} \cdot \text{H}_2\text{O}$	1582 s	1352 m	230
MnL.2.5H ₂ O	1560 s	1372 m	188
FeL.2.5H ₂ O	1564 s	1380 m	184
CoL.2H ₂ O	1562 s	1368 m	194
NiL.2H ₂ O	1559 s	1376 m	183
CuL.2H ₂ O	1576 s	1372 m	204
ZnL.2H ₂ O	1563 s	1368 m	195

L = malonate; s = strong; m = medium; $\nu_{\text{as}}(\text{COO}^-)$ and $\nu_{\text{sym}}(\text{COO}^-)$: anti-symmetrical and symmetrical vibrations of the COO^- group, respectively.

1700–1400 cm^{-1} range because this region is potentially most informative in attempting to assign coordination sites.

In $\text{Na}_2\text{CH}_2\text{C}_2\text{O}_4$, strong band at 1582 cm^{-1} and a medium intensity band located at 1352 cm^{-1} are attributed to the anti-symmetrical and symmetrical frequencies of the carboxylate groups, respectively. The band assigned to the anti-symmetrical stretching carboxylate frequencies are shifted to lower values relative to the corresponding frequencies in $\text{CH}_2\text{C}_2\text{O}_4$ itself (sodium salt). This behaviour indicates that the coordination carried out through the carboxylate group [17] and the infrared spectra data suggests that the bonding of the carboxylate group to the metal is chelating bidentate and/or bridging in these compounds [18,19]. This conclusion is supported (at least in the case of the Cu and Zn compound) by the results of the crystal structure determination of Cu malonate trihydrate [20] and Zn malonate dihydrate [21].

Simultaneous TG-DTA and DSC curves of the compounds are shown in Fig. 4. The TG-DTA curves show mass losses or gain in

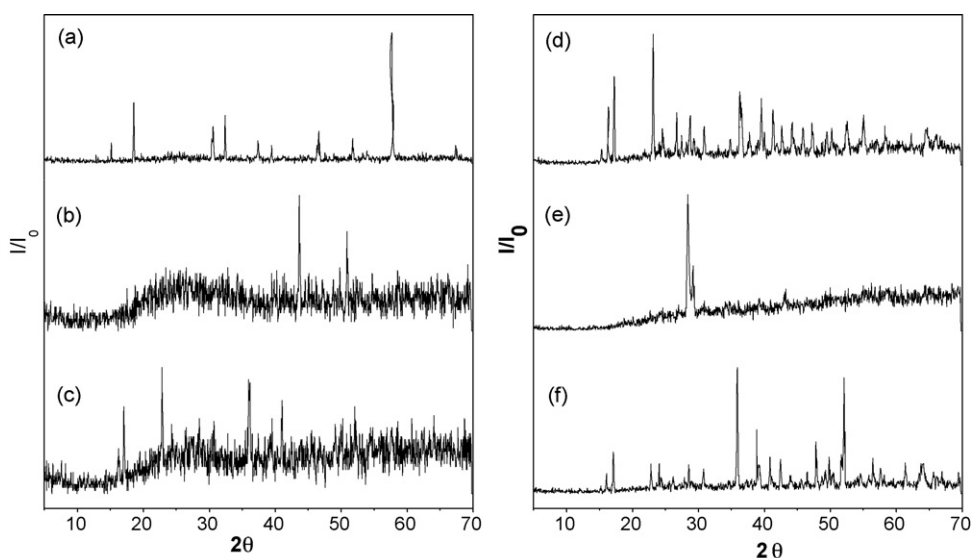


Fig. 3. X-ray powder diffraction patterns of the compounds: (a) MnL.2.5H₂O, (b) FeL.2.5H₂O, (c) CoL.2H₂O, (d) NiL.2H₂O, (e) CuL.2H₂O and (f) ZnL.2H₂O. (L = malonate).

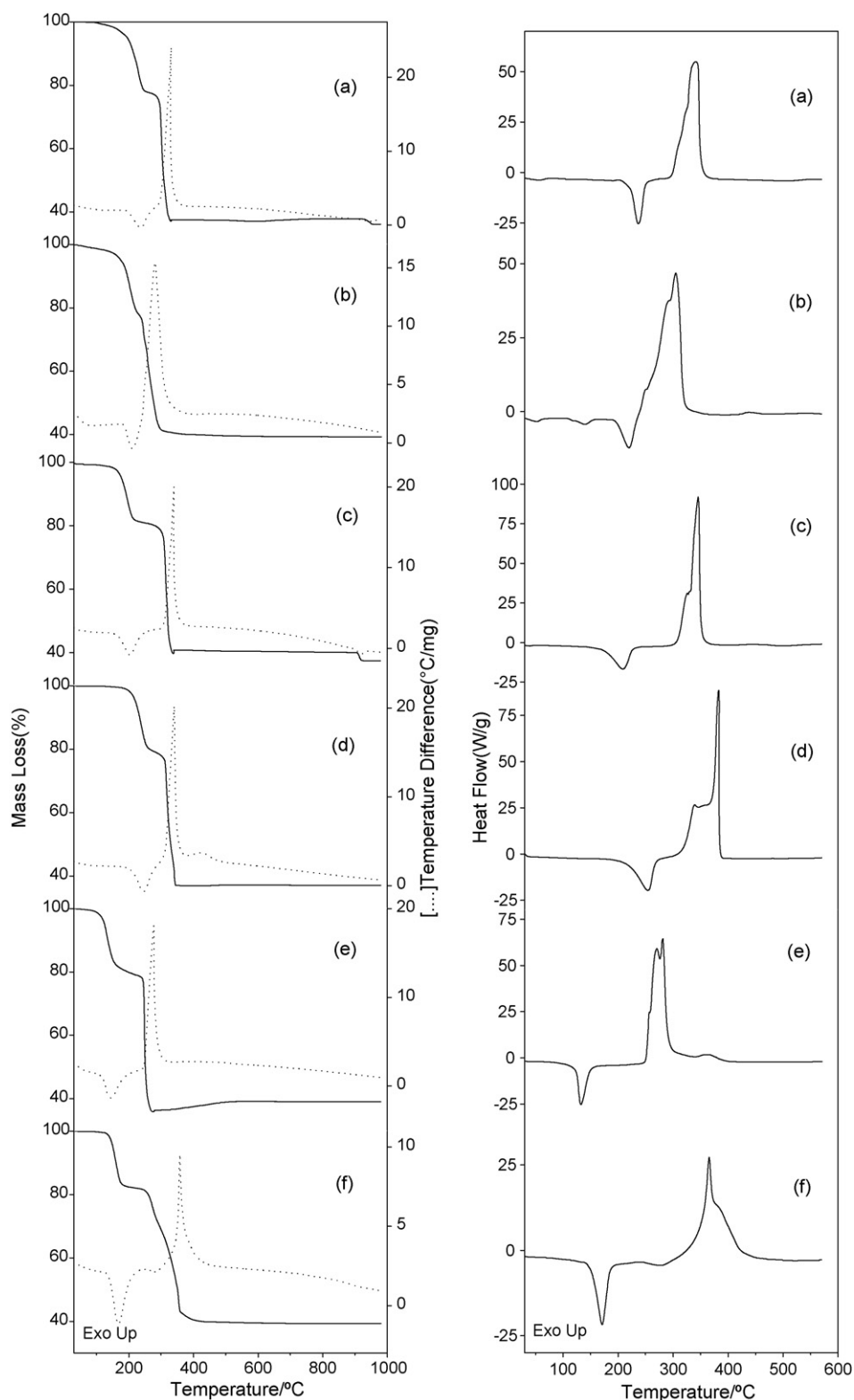


Fig. 4. Simultaneous TG-DTA and DSC curves of the compounds: (a) $\text{MnL}_2 \cdot 2.5\text{H}_2\text{O}$ ($m = 7.441$ and 2.032 mg), (b) $\text{FeL}_2 \cdot 2.5\text{H}_2\text{O}$ (7.327 and 2.011 mg), (c) $\text{CoL}_2 \cdot 2\text{H}_2\text{O}$ (7.424 and 2.034 mg), (d) $\text{NiL}_2 \cdot 2\text{H}_2\text{O}$ (7.232 and 2.021 mg), (e) $\text{CuL}_2 \cdot 2\text{H}_2\text{O}$ (7.151 and 2.028 mg) and (f) $\text{ZnL}_2 \cdot 2\text{H}_2\text{O}$ (7.182 and 2.055 mg).

two or three steps, corresponding to endothermic peak due to dehydration or reduction reaction and exothermic peaks attributed to oxidation of organic matter. The DSC curves also show endothermic and exothermic peaks corresponding to the mass losses displayed by the TG curves. The differences observed concerning the peak temperatures obtained by TG-DTA and DSC curves, and the profiles

of the DTA and DSC ones are undoubtedly due to the perforated cover used to obtain the DSC curves, while the TG-DTA ones are obtained without cover; in addition to the experimental conditions were not the same, too.

The thermal stability of the hydrated (I) or anhydrous compounds (II), as well as the final temperature of thermal decom-

position (III) as shown by TG-DTA curves depend on the nature of the metal ion, and they follow the order:

I : Ni > Co > Zn > Mn > Cu > Fe

II : Ni > Mn > Co > Fe = Zn > Cu

III : Zn > Fe > Ni > Co > Mn > Cu

The TG-DTA curves also show that the formation of stable anhydrous compounds is observed for manganese, cobalt and zinc compounds, while for iron, nickel and copper ones the thermal decomposition occurs immediately after the dehydration.

The thermal behaviour of the compounds is heavily dependent on the nature of the metal ion and so the features of each these compounds are discussed individually.

3.1. Manganese compound

The simultaneous TG-DTA and DSC curves are shown in Fig. 4(a). The first mass loss observed between 100 and 255 °C (TG), corresponding to an endothermic peak at 240 °C (DTA) and 238 °C (DSC) is due to dehydration with loss of 2.5 H₂O (Calcd. = 22.30%, TG = 22.14%). The thermal decomposition of the anhydrous compounds occurs in a single step, between 270 and 335 °C with loss of 39.95%, corresponding to the exothermic peak at 335 °C (DTA) and 341 °C (DSC), which are attributed to the oxidation of the organic matter. The total mass loss up to 335 °C is in agreement with the formation of Mn₃O₄ (Calcd. = 62.25%, TG = 62.45%). The last mass loss observed between 920 and 955 °C is assigned to the reduction of Mn₃O₄ to MnO (Calcd. = 2.64%, TG = 1.65%), in agreement with the literature [22].

3.2. Iron compound

The simultaneous TG-DTA and DSC curves are shown in Fig. 4(b). The first mass loss observed between 50 and 230 °C (TG), corresponding to endothermic peak at 210 °C (DTA) or 55, 140 and 220 °C (DSC) is due to dehydration with loss of 2.5 H₂O (Calcd. = 22.20%, TG = 21.87%). Immediately after the dehydration, the anhydrous compound shows mass loss in a single step between 230 and 400 °C with loss of 39.05%, corresponding to the exothermic peak at 280 °C (DTA) and 305 °C with shoulder at 251 and 293 °C (DSC), attributed to the oxidation of Fe(II) to Fe(III) and organic matter. The total mass loss up to 400 °C is in agreement with the formation of Fe₂O₃ as final residue (Calcd. = 60.66%, TG = 60.92%), which was confirmed by X-ray powder diffractometry.

3.3. Cobalt compound

The simultaneous TG-DTA and DSC curves are shown in Fig. 4(c). The first mass loss that occurs between 130 and 235 °C (TG), corresponding to endothermic peak at 205 °C (DTA) or 209 °C (DSC) is due to dehydration with loss of 2H₂O (Calcd. = 18.29%, TG = 17.98%). The thermal decomposition of the anhydrous compound occurs in a single step between 250 and 340 °C with loss of 41.58%, corresponding to exothermic peak at 340 °C (DTA) or 345 °C with shoulder at 328 °C (DSC), attributed to oxidation of the organic matter. The total mass loss up to 340 °C is in agreement with the formation of Co₃O₄ (Calcd. = 59.26%, TG = 59.56%). The last mass loss that occurs between 905 and 925 °C, corresponding to the endothermic peak at 915 °C (DTA) is attributed to reduction of Co₃O₄ to CoO (Calcd. = 2.71%, TG = 2.78%) in agreement with the literature [23–24]. The X-ray powder pattern of the residue obtained at 950 °C is coincident with that one obtained for Co₃O₄; this is due to the

oxidation reaction of CoO to Co₃O₄, which occurs on cooling the former in an air atmosphere at room temperature [23,25].

3.4. Nickel compound

The simultaneous TG-DTA and DSC curves are shown in Fig. 4(d). The mass loss that occurs between 160 and 275 °C, corresponding to endothermic peak at 245 °C (DTA) or 254 °C (DSC), is due to dehydration with loss of 2H₂O (Calcd. = 18.31%, TG = 18.55%). After the dehydration the thermal decomposition occurs in a single step, where the mass loss begins with a slow process, followed by a fast one, between 275 and 350 °C with loss of 43.69%. This mass loss corresponds to exothermic peak at 340 °C (DTA) or 339 and 382 °C (DSC) attributed to oxidation of the organic matter. The total mass loss up to 350 °C is in agreement with the formation of NiO as final residue (Calcd. = 62.04%, TG = 62.24%) and confirmed by X-ray powder diffractometry.

3.5. Copper compound

The simultaneous TG-DTA and DSC curves are shown in Fig. 4(e). The mass loss observed between 75 and 200 °C (TG), corresponding to endothermic peak at 145 °C (DTA) or 132 °C (DSC) is due to dehydration with loss of 2H₂O (Calcd. = 17.87%, TG = 17.63%). After the dehydration the thermal decomposition begins through a slow process, followed by a fast one between 200 and 275 °C with loss of 46.40% corresponding to exothermic peak at 275 °C (DTA) or the exotherm with two peaks at 271 and 281 °C (DSC) attributed to oxidation of organic matter. The mass loss up to 275 °C is in agreement with the formation of the Cu₂O as residue (Calcd. = 64.52%, TG = 64.03%). The mass gain that occurs between 275 and 520 °C, corresponding to exothermic peak at 364 °C is attributed to the oxidation of Cu(I) to Cu(II) with formation of CuO as final residue (Calcd. = 60.55%, TG = 60.94%), which was confirmed by X-ray powder diffractometry.

3.6. Zinc compound

The TG-DTA and DSC curves are shown in Fig. 4(f). The mass loss observed between 110 and 190 °C (TG), corresponding to the exothermic peak at 170 °C (DTA) or 171 °C (DSC) is due to dehydration with loss of 2H₂O (Calcd. = 17.71%, TG = 17.55%). The anhydrous compound is stable up to 230 °C and above this temperature the thermal decomposition occurs between 230 and 450 °C with loss of 42.70%, corresponding to exothermic peak at 355 °C (DTA) or 366 °C (DSC) attributed to oxidation of organic matter. The total mass loss up to 450 °C is in agreement with the formation of ZnO as final residue (Calcd. = 60.01%, TG = 60.25%), which was confirmed by X-ray powder diffractometry.

The dehydration temperatures, thermal stability of the anhydrous compounds, as well as the minimum oxide level temperatures observed in the present paper are in disagreement with the results reported by Randhawa and Gandotra [13], even the final residue MnO and CoO for the manganese and cobalt compounds, respectively. These disagreements undoubtedly are due to the static air atmosphere used to obtain the TG and DTA curves in the work of Ref. [13], while dynamic air atmosphere was used in the present paper.

It is well known that the experimental conditions affect the TG and DTA curves. For the dynamic atmosphere the evolved products of the thermal decomposition are continuously changed while in the static atmosphere the same is not observed. On that account the disagreements are observed.

The gaseous products evolved during the thermal decomposition of the sodium and transition metal-ion compounds studied in

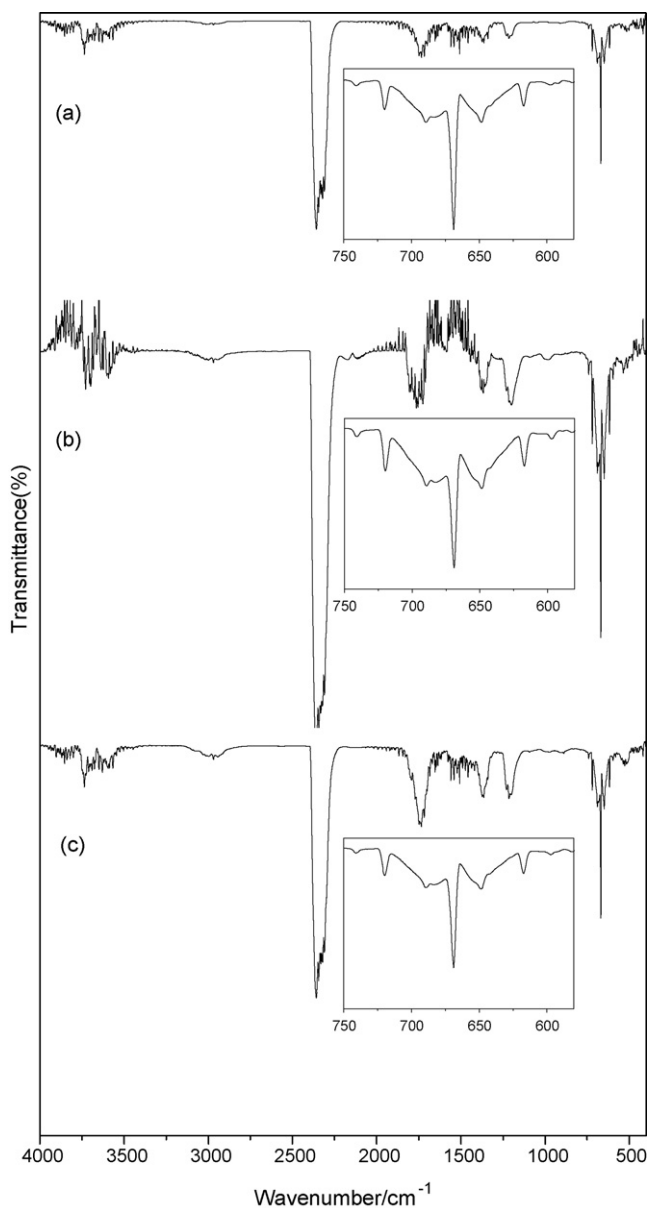


Fig. 5. IR spectra of gaseous products evolved during the decomposition of the compounds: (a) $\text{Na}_2\text{L}\cdot\text{H}_2\text{O}$, (b) $\text{CoL}\cdot 2\text{H}_2\text{O}$ (c) $\text{ZnL}\cdot 2\text{H}_2\text{O}$. L = malonates.

this work were monitored by FTIR, and it has carbon dioxide as main product due to the decarboxylation and oxidation of organic matter. The IR spectra of the gaseous products evolved during the thermal decomposition of sodium, cobalt and zinc malonates, as representative of all the compounds are shown in Fig. 5. Some overlapping bands of low intensity between 1780 and 1700 cm^{-1} , 1380 and 1340 cm^{-1} and 1240 and 1187 cm^{-1} suggesting the presence of $-\text{C}=\text{O}$, $-\text{CH}_2-$ and $-\text{CH}_3$, $\text{C}-\text{C}$ and/or $-\text{C}-\text{O}$ groups, respectively. A peak at 720 cm^{-1} which is observed only for $-\text{CH}_2-$ vibration (rocking) in the molecule confirms that the decomposition

is accompanied by small parallel reactions with formation of new gaseous products.

4. Conclusion

From TG, complexometry and elemental analysis data, a general formula could be established for the binary compounds involving some bivalent metal ions and $\text{CH}_2\text{C}_2\text{O}_4$. The X-ray powder patterns pointed out that the synthesized compounds have a crystalline structure with evidence concerning the formation of isomorphous compounds only for cobalt and nickel ones.

The infrared spectroscopic data suggests that $\text{CH}_2\text{C}_2\text{O}_4$ acts as a chelating bidentate and/or bridging bidentate ligand towards the metal ions considered in this work.

The TG-DTA and DSC curves provided previously unreported information about the thermal stability and thermal decomposition of these compounds in dynamic air atmosphere.

The monitoring of evolved gases showed that the degradation of malonic acid occurs with decarboxylation followed by acetic acid formation. The thermal decomposition of metal malonates occurred preferentially with the release of carbon dioxide due to decarboxylation and oxidation of organic matter.

Acknowledgements

The authors thank FAPESP, CNPq and CAPES Foundations for financial support. This work is funded by BZG.

References

- [1] H.-Y. Shen, W.-M. Bu, D.-Z. Liao, J.-H. Jiang, S.P. Yan, G.-L. Wang, *Inorg. Chem. Commun.* 3 (2000) 497–500.
- [2] Y. Rodriguez-Martin, C. Ruiz-Pérez, J. Sanchiz, F. Lloret, M. Julve, *Inorg. Chim. Acta* 318 (2001) 159–165.
- [3] Y. Rodriguez-Martin, M. Hernandez-Molina, F.S. Delgado, J. Pasan, C. Ruiz-Perez, J. Sanchiz, F. Lloret, M. Julve, *Cryst. Eng. Commun.* 4 (2002) 522–535.
- [4] K. Muraishi, K. Nagase, *Thermochim. Acta* 159 (1990) 225–233.
- [5] K. Muraishi, *Thermochim. Acta* 164 (1990) 401–409.
- [6] K. Nagase, H. Yokobayashi, K. Muraishi, M. Kikuchi, *Thermochim. Acta* 177 (1991) 273–284.
- [7] Y. Suzuki, *Thermochim. Acta* 255 (1995) 155–170.
- [8] K. Muraishi, Y. Suzuki, Y. Takahashi, *Thermochim. Acta* 286 (1996) 187–198.
- [9] A.K. Galwey, S.G. McKee, T.R.B. Mitchell, M.A. Mohamed, M.E. Brown, A.F. Bean, *Reactivity Solids* 6 (1988) 187–203.
- [10] M.A. Mohamed, A.K. Galwey, S.A. Halawy, *Thermochim. Acta* 323 (1998) 27–36.
- [11] M.A. Mohamed, A.K. Galwey, S.A. Halawy, *Thermochim. Acta* 346 (2000) 91–103.
- [12] M.A. Mohamed, S.A. Halawy, *J. Anal. Appl. Pyrol.* 80 (2007) 238–246.
- [13] B.S. Randhawa, K. Gandotra, *J. Therm. Anal. Calorim.* 85 (2) (2006) 417–424.
- [14] H.A. Flaschka, *EDTA Titrations*, Pergamon Press, Oxford, 1964.
- [15] C.N. de Oliveira, M. Ionashiro, C.A.F. Graner, *Ecl. Quim.* 10 (1985) 7–10.
- [16] JCPDS-ICDD, PDF2 Data Base (1996).
- [17] K. Nakamoto, *Infrared and Raman Spectra of Inorganic and Coordination Compounds Part B*, 5th ed., Wiley, New York, 1997, pp. 58–61.
- [18] G.B. Deacon, R.J. Phillips, *Coord. Chem. Rev.* 33 (1980) 227–250.
- [19] R.I. Bickley, H.G.M. Edwards, A. Knowles, R.E. Gustar, D. Mihara, S.J. Rose, *J. Mol. Struct.* 296 (1993) 21–28.
- [20] P. Naumov, M. Ristova, B. Soptrajanov, M.G.B. Drew, S.W. Ng, *Croat. Chem. Acta* 75 (2002) 701–711.
- [21] Z.L. Wang, L.H. Wei, J.Y. Niu, *Acta Cryst. E* 61 (2005) 1907–1908.
- [22] L. Biernacki, S. Pokrzywnicki, *J. Therm. Anal. Calorim.* 55 (1999) 227–232.
- [23] G.A. El-Shobaky, A.S. Ahmad, A.N. Al Noaim, H.G. El-Shobaky, *J. Therm. Anal.* 46 (1996) 1801–1808.
- [24] G. Bannach, A.B. Siqueira, E.Y. Ionashiro, E.C. Rodrigues, M. Ionashiro, *J. Therm. Anal. Calorim.* 90 (3) (2007) 873–879.
- [25] Z.P. Xu, H.C. Zeng, *J. Mater. Chem.* 8 (11) (1998) 2499–2506.